Physics of Plasmas ARTICLE scitation.org/journal/php

Mapping for nonlinear electron interaction with whistler-mode waves

Cite as: Phys. Plasmas **27**, 042902 (2020); doi: 10.1063/1.5144477
Submitted: 5 January 2020 · Accepted: 17 March 2020 ·
Published Online: 10 April 2020

A. V. Artemyev,[1,a] A. I. Neishtadt,[2,b] and A. A. Vasiliev[3,c]

AFFILIATIONS

[1]Institute of Geophysics and Planetary Physics, UCLA, Los Angeles, California 90095-1567, USA
[2]Department of Mathematical Sciences, Loughborough University, Loughborough LE11 3TU, United Kingdom
[3]Space Research Institute of the Russian Academy of Sciences (IKI), 84/32 Profsoyuznaya Str., Moscow 117997, Russia

[a]**Also:** Space Research Institute of the Russian Academy of Sciences (IKI), 84/32 Profsoyuznaya Str., Moscow 117997, Russia. **Author to whom correspondence should be addressed:** aartemyev@igpp.ucla.edu
[b]**Also:** Space Research Institute of the Russian Academy of Sciences (IKI), 84/32 Profsoyuznaya Str., Moscow 117997, Russia. **Electronic mail:** a.neishtadt@lboro.ac.uk
[c]**Electronic mail:** valex@iki.rssi.ru

ABSTRACT

The resonant interaction of relativistic electrons and whistler-mode waves is an important mechanism of electron acceleration and scattering in the Earth radiation belts and other space plasma systems. For low amplitude waves, such an interaction is well described by the quasi-linear diffusion theory, whereas nonlinear resonant effects induced by high-amplitude waves are mostly investigated (analytically and numerically) using the test particle approach. In this paper, we develop a mapping technique for the description of this nonlinear resonant interaction. Using the Hamiltonian theory for resonant systems, we derive the main characteristics of electron transport in the phase space and combine these characteristics to construct the map. This map can be considered as a generalization of the classical Chirikov map for systems with nondiffusive particle transport and allows us to model the long-term evolution of the electron distribution function.

I. INTRODUCTION

Whistler-mode waves are electromagnetic emissions within the frequency range from the lower-hybrid up to electron cyclotron frequency widely observed in space[1,52,88,103,105] and laboratory[76,92] plasmas. These waves are generated by various types of electron distributions with thermal anisotropy,[43,96] beam distributions,[9,47,100,101] or both,[10,54,57] and they play an important role in the isotropisation of originally unstable electron distributions.[33,49,82] A classical theory of whistler-mode resonant interaction with electrons is the quasi-linear theory[42,51,97] that assumes a broad spectrum of low amplitude waves. This theory allows us to describe the main characteristics of electron acceleration[53,85] and scattering[64,86] in the Earth radiation belts, in the solar wind,[71] and at the Earth bow shock.[98,99] However, quasi-linear theory cannot describe resonant interactions with the very intense coherent waves[38,79] often observed in space plasmas.[2,87,90,102,103,106,107] Such sufficiently intense whistler-mode waves can resonate nonlinearly with electrons.[23,39,65] Such nonlinear interaction can lead to phase trapping or non-diffusive scattering of particles[6,75] and can result in a very fast electron acceleration.[7,28,29,31,34,67,81,104] Therefore, the effects of nonlinear resonant interaction are actively investigated (see reviews in Refs. 8, 10, 14, 68, and 73).

Since self-consistent Vlasov or particle-in-cell simulations of whistler-mode wave generation and their resonances with electrons[30,40,48,83] can hardly cover the long-term dynamics of the electron distribution in realistic space plasma systems, alternative approaches need to be considered. Besides the test particle approach (i.e., the numerical integration of a large number of electron trajectories[4,46,66]), the most interesting approach for the investigation of nonlinear electron resonances with whistler-mode waves consists of the derivation of a kinetic equation (master-equation[93]) describing the evolution of the electron distribution. This approach generalizes the quasi-linear diffusion equation by including terms responsible for electron nonlinear acceleration and scattering.[15,20,31,69] Such terms can be derived analytically[17,91] or numerically.[35,36,69]

A less investigated but potentially useful approach is the mapping technique already widely used for systems with small wave

amplitudes.[55,70] The well-known Chirikov map[27] describes phase space diffusion and transport induced by periodical random jumps of particle momentum. The resonance of electrons and whistler-mode waves results in a similar type of dynamics: each resonant interaction corresponds to an electron energy (and pitch-angle) jump inducing particle transport in phase space. For small amplitude whistler-mode waves, the map of electron resonant jumps is quite similar to the Chirikov map,[24,44,45] but nonlinear resonant interaction should significantly change such a map. In this study, we develop a map describing electron motion in a system with multiple passages through nonlinear resonances. We have also demonstrated that this map models well the electron distribution evolution and can be used to study the radiation belt dynamics.

II. BASIC EQUATIONS

To derive the basic properties of the nonlinear electron (m_e is the rest mass and $-e$ is the charge) interaction with a single field-aligned whistler-mode wave [ω is a constant frequency, $k(\omega, s)$ is the wave number given by the cold plasma dispersion relation[77] and depends on the field-aligned coordinate s], we consider the Hamiltonian of electron motion $\sqrt{m_e^2c^4 + p_\parallel^2c^2 + 2I_x\Omega_{ce}m_ec^2}$ and a small perturbation by wave-field (i.e., we consider waves with the wave field energy much smaller than m_ec^2, see details in, e.g., Refs. 18 and 91),

$$H = m_ec^2\gamma + U_w(s, I_x)\sin(\phi + \psi),$$
$$\gamma = \sqrt{1 + \frac{p_\parallel^2}{m_e^2c^2} + \frac{2I_x\Omega_{ce}}{m_ec^2}}, \tag{1}$$

where c is the speed of light, γ is the Lorentz factor of the gyroaveraged system, $\Omega_{ce} = eB_0(s)/m_ec$ is the electron gyrofrequency in the background magnetic field $B_0(s)$ given by the reduced dipole model,[23] $U_w = \sqrt{2I_x\Omega_{ce}m_e}eB_w/\gamma m_ec k$ with B_w the wave amplitude, and I_x is the magnetic moment normalized in a such a way that $I_x\Omega_{ce}$ has the dimension of energy. The conjugate pairs of variables in Eq. (1) are field-aligned coordinate and momentum, $(s, p_\parallel)$, and gyrophase and magnetic moment, ψ, I_x. Hamiltonian (1) can be derived from the Hamiltonian of 3D charged particle motion with two key assumptions: (1) the background magnetic field is sufficiently strong to magnetize electron and allows introduction of magnetic moment I_x, which is conserved in the absence of wave (note magnetic moment is conjugate to the gyrophase ψ, and I_x introduction results in two Hamiltonian equations: $\dot{I}_x = -\partial H/\partial\psi$, $\dot{\psi} = \partial H/\partial I_x$, see Ref. 50) and (2) wave field energy is much smaller than m_ec^2, and thus wave field can be considered as a perturbation in the Hamiltonian (see details of these derivations in, e.g., reviews of Refs. 8, 14, and 73). Note that Hamiltonian (1) is written for electrons interacting with field-aligned whistler-mode waves, i.e., only $n = -1$ cyclotron resonance is available, and this defines that wave field depends on $\phi + \psi$ (see more general form of this Hamiltonian in, e.g., Refs. 8, 18, and 73).

Wave phase ϕ is given by the differential equation: $\dot{\phi} = k(s)\dot{s} - \omega$ (we omit the argument ω in the function k). In system (1) phases ϕ, ψ changes much faster than variables $s, p_\parallel$, and I_x because wave frequency ω and gyrofrequency Ω_{ce} are much larger than the electron bounce frequency $\sim c/R$ where R is a spatial scale of $B_0(s)$ gradient. Therefore, the first small parameter of the system is $c/R\Omega_{ce} \ll 1$. The second small parameter of the system is $B_w/B_0 \ll 1$, and we consider sufficiently intense waves with $B_w/B_0 \geq c/R\Omega_{ce}$ (this condition is satisfied for a significant fraction of whistler-mode waves observed in the Earth radiation belts, see Ref. 107).

Figure 1(a) shows several fragments of electron trajectories around the resonance $\dot{\phi} + \dot{\psi} = 0$ (with $\dot{\psi} = \partial H/\partial I_x \approx \Omega_{ce}/\gamma$): there are two main effects[63]—electron trapping into resonance with the energy increase $\Delta\gamma_{trap}$, and electron scattering on the resonance with the energy decrease $\Delta\gamma_{scat}$. We plan to construct a map describing the long-term evolution produced by these two processes.

We start with the determination of $\Delta\gamma_{trap}$, $\Delta\gamma_{scat}$ and their dependencies on particle characteristics. First, we use the generating function,

$$W_1 = \left(\left(\int k(\tilde{s})d\tilde{s} - \omega t\right) + \psi\right)I + sP,$$

to introduce phase $\varphi = \phi + \psi$ and conjugate momentum I,

$$H_I = -\omega I + m_ec^2\gamma + U_w(s, I)\sin\varphi,$$
$$\gamma = \sqrt{1 + \frac{(P + kI)^2}{m_e^2c^2} + \frac{2I\Omega_{ce}}{m_ec^2}}. \tag{2}$$

Pairs of conjugate variables are (I, φ) and (s, P) with $P = p_\parallel - kI$. The resonance condition ($\dot{\varphi} = \partial H_I/\partial I = 0$) for Hamiltonian (2) defines the resonant momentum $I_R(s, P)$,

$$\frac{kI_R}{m_ec} = \sqrt{\frac{1 - (\Omega_{ce}/kc)^2 - 2\left(\Omega_{ce}P/km_ec^2\right)}{(kc/\omega)^2 - 1}} - \frac{\Omega_{ce}}{kc} - \frac{P}{m_ec}. \tag{3}$$

We expand Hamiltonian (2) around the resonance,

$$H_I \approx \Lambda + \frac{1}{2}g(I - I_R)^2 + U_w(s, I_R)\sin\varphi,$$
$$\Lambda = -\omega I_R + m_ec^2\gamma_R, \quad \gamma_R = \sqrt{1 + \frac{(P + kI_R)^2}{m_e^2c^2} + \frac{2I_R\Omega_{ce}}{m_ec^2}},$$
$$g = m_ec^2\frac{\partial^2\gamma}{\partial I^2}\bigg|_{I=I_R} = \frac{\omega^2\left((kc/\omega)^2 - 1\right)}{\gamma_R}, \tag{4}$$

and use the generating function,

$$W_2 = (I - I_R)\zeta + Ps^*,$$

to introduce new pairs of conjugate variables (ζ, P_ζ) and (s^*, P^*) with $P_\zeta = I - I_R$, $s^* = s + (\partial I_R/\partial P)\zeta$, $P^* = P - (\partial I_R/\partial s)\zeta$, $\zeta = \varphi$,

$$\tilde{H}_I = \Lambda(s^*, P^*) + \frac{1}{2}gP_\zeta^2 + U_w(s, I_R)\sin\zeta$$
$$\approx \Lambda(s, P) + \frac{1}{2}gP_\zeta^2 - r\zeta + U_w(s, I_R)\sin\zeta,$$
$$r = \{\Lambda, I_R\}_{s,P} = \frac{\partial\Lambda}{\partial s}\frac{\partial I_R}{\partial P} - \frac{\partial\Lambda}{\partial P}\frac{\partial I_R}{\partial s}. \tag{5}$$

Using Hamiltonian (2), we get $m_ec^2\Delta\gamma = \omega\Delta I$ (note $\partial H_I/\partial t = 0$) and $\dot{I} = -\partial H_I/\partial\varphi = -U_w\cos(\varphi)$, i.e., there is a conserved energy $h = -\omega I + m_ec^2\gamma$. Therefore, the energy change $\Delta\gamma$ due to resonant interaction can be written as[14,62]

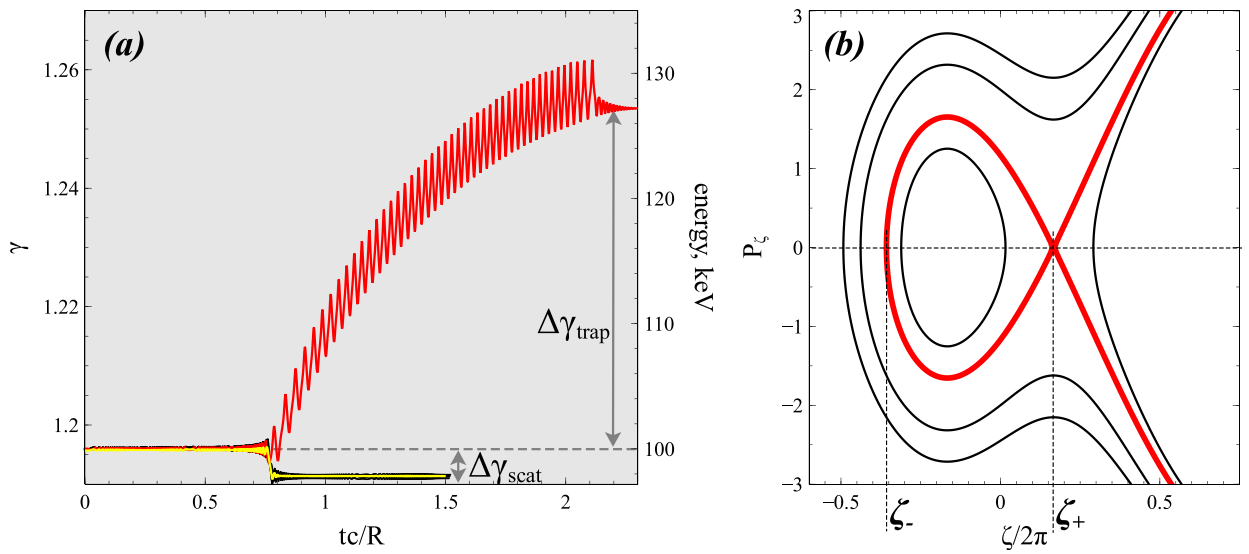

FIG. 1. (a) Change of electron energy due to scattering (black; yellow shows averaged energy of scattered particles) and trapping (red). The time interval of one resonant interaction is shown. All electrons have initially the same energy and pitch-angle. For these trajectories and throughout the paper, we consider a curvature-free dipole magnetic field[23] with the radial distance from the Earth $R = 4.5$ of the Earth radii. The whistler-mode wave frequency is 0.35 times the electron cyclotron frequency at the equator, and plasma frequency equals to 4.5 of the electron cyclotron frequency at the equator. To evaluate the wave number k, we use the cold plasma dispersion of whistler-mode waves.[77] The wave amplitude is 300 pT, typical for intense whistler-mode waves observed in the radiation belts.[26,90,102,106] The distribution of the wave amplitude along magnetic field lines, $B_w(s)$, is modeled by function $\tanh((\lambda/\delta\lambda_1)^2)\exp(-(\lambda/\delta\lambda_2)^2)$ with λ the magnetic latitude ($ds = Rd\lambda\sqrt{1+\sin^2\lambda}\cos\lambda$) and $\delta\lambda_1 = 2^\circ$, $\delta\lambda_2 = 20^\circ$. This function fits the observed whistler-mode wave intensity distribution.[1] To simplify the simulations, we consider waves in only one hemisphere, $B_w = 0$ for $s < 0$, and thus, there is only one resonance for electrons within one bounce period. Waves are moving away from the equatorial plane, $s = 0$, to large s, i.e., only $k > 0$ are included. (b) Phase portrait of Hamiltonian $\tilde{H}_I - \Lambda = gP_\zeta^2/2 - r\zeta + U_w \sin\zeta$ for $|U_w/r| > 1$.

$$
\begin{aligned}
m_e c^2 \Delta\gamma &= -\omega U_w \int_{-\infty}^{+\infty} \cos\varphi dt = -2\omega U_w \int_{t_R}^{+\infty} \cos\varphi dt, \\
&= -2\omega U_w \int_{\zeta_R}^{+\infty} \frac{\cos\zeta}{gP_\zeta} d\zeta = -\sqrt{\frac{2}{g}}\omega \int_{\zeta_R}^{+\infty} \frac{U_w \cos\zeta d\zeta}{\sqrt{h_\zeta + r\zeta - U_w \sin\zeta}}, \\
&= -\sqrt{\frac{2U_w}{g}}\omega \int_{\zeta_R}^{+\infty} \frac{a\cos\zeta d\zeta}{\sqrt{(\zeta-\zeta_R) - a(\sin\zeta - \sin\zeta_R)}}, \\
&= -\sqrt{\frac{2r}{g}}\omega f(\zeta_R, a), \qquad (6)
\end{aligned}
$$

where t_R is the time of the resonant interaction, ζ_R is the value of ζ at $t = t_R$, and we use the Hamiltonian equation $\dot{\zeta} = \partial\tilde{H}_I/\partial P_\zeta$ to express P_ζ through the energy at the resonance $h_\zeta = \tilde{H}_I - \Lambda = U_w \sin\zeta_R - r\zeta_R$ [note that Eq. (6) is written for $r > 0$, whereas for $r < 0$, the ζ-integration would be from $-\infty$ to ζ_r, see details in Refs. 14 and 62]. Coefficient $a = U_w/r$ determines the mode of resonant interaction: for $|a| > 1$ we deal with nonlinear interaction with $\langle\Delta\gamma\rangle_{h_\zeta} \neq 0$, where $\langle\cdot\rangle_{h_\zeta}$ denotes averaging with respect to h_ζ. Function $f(\zeta_R, a)$ is shown in Fig. 2(a). This is a periodic function with the average value[14,62] equal to

$$
\langle\Delta\gamma\rangle_{h_\zeta} = \frac{\omega}{\pi}\sqrt{\frac{2r}{g}} \int_{\zeta_-}^{\zeta_+} \sqrt{(\zeta-\zeta_-) - a(\sin\zeta - \sin\zeta_-)} d\zeta, \qquad (7)
$$

where $\zeta_\pm$ are shown in the phase portrait of the Hamiltonian $\tilde{H}_I - \Lambda$ [see Fig. 1(b)]. Note that we consider only systems with sufficiently high-amplitude waves (for which $|a| > 1$ and $\langle\Delta\gamma\rangle \neq 0$), whereas for low-amplitude waves $\langle\Delta\gamma\rangle = 0$ and there is only diffusion $\sim\langle(\Delta\gamma)^2\rangle$ due to scattering (see Refs. 24, 44, and 45).

The energy change in Eq. (7) represents the energy scattering $\Delta\gamma_{scat} = \langle\Delta\gamma\rangle_{h_\zeta}$ and depends on the resonance position s_R given by the following equations:

$$
h = -\omega I_R(s, P) + m_e c^2 \gamma_R(s, P), \quad \gamma_0 = \gamma_R(s, P), \qquad (8)
$$

where $m_e c^2 \gamma_0$ is the initial electron energy and h can be written as $h = -\omega I_{x0} + m_e c^2 \gamma_0$ (with I_{x0} being the initial I_x value). Equation (8) can be rewritten as

$$
\gamma_R = \left| \frac{\Omega_{ce}}{kc} \mp \frac{kc}{\sqrt{(kc)^2 - \omega^2}} \sqrt{1 + \left(\frac{\Omega_{ce}}{kc}\right)^2 - \frac{2h}{m_e c^2}\frac{\Omega_{ce}}{kc}} \right|. \qquad (9)
$$

Figure 2(b) shows the profile of $\Delta\gamma_{scat}$ along the magnetic field line (we use magnetic latitude λ instead of coordinate s, i.e., λ_R is the solution of equation $s_R/R = \int_0^{\lambda_R} d\lambda\sqrt{1+\sin^2\lambda}\cos\lambda$). For a given h (or equivalently for a given initial pitch-angle α_0 determining I_{x0}), we can plot $\Delta\gamma_{scat}$ as a function of initial energy $m_e c^2 \gamma_0$, see Fig. 2(c). As h is determined by α_0 and γ_0, the energy scattering value $m_e c^2 \Delta\gamma_{scat}$ depends on α_0, γ_0. Analogous dependencies of scattering on initial particle parameters have been tested for several specific Hamiltonians.[17,21,91] For Hamiltonian (1), we compare the numerically calculated $\Delta\gamma_{scat}$ with

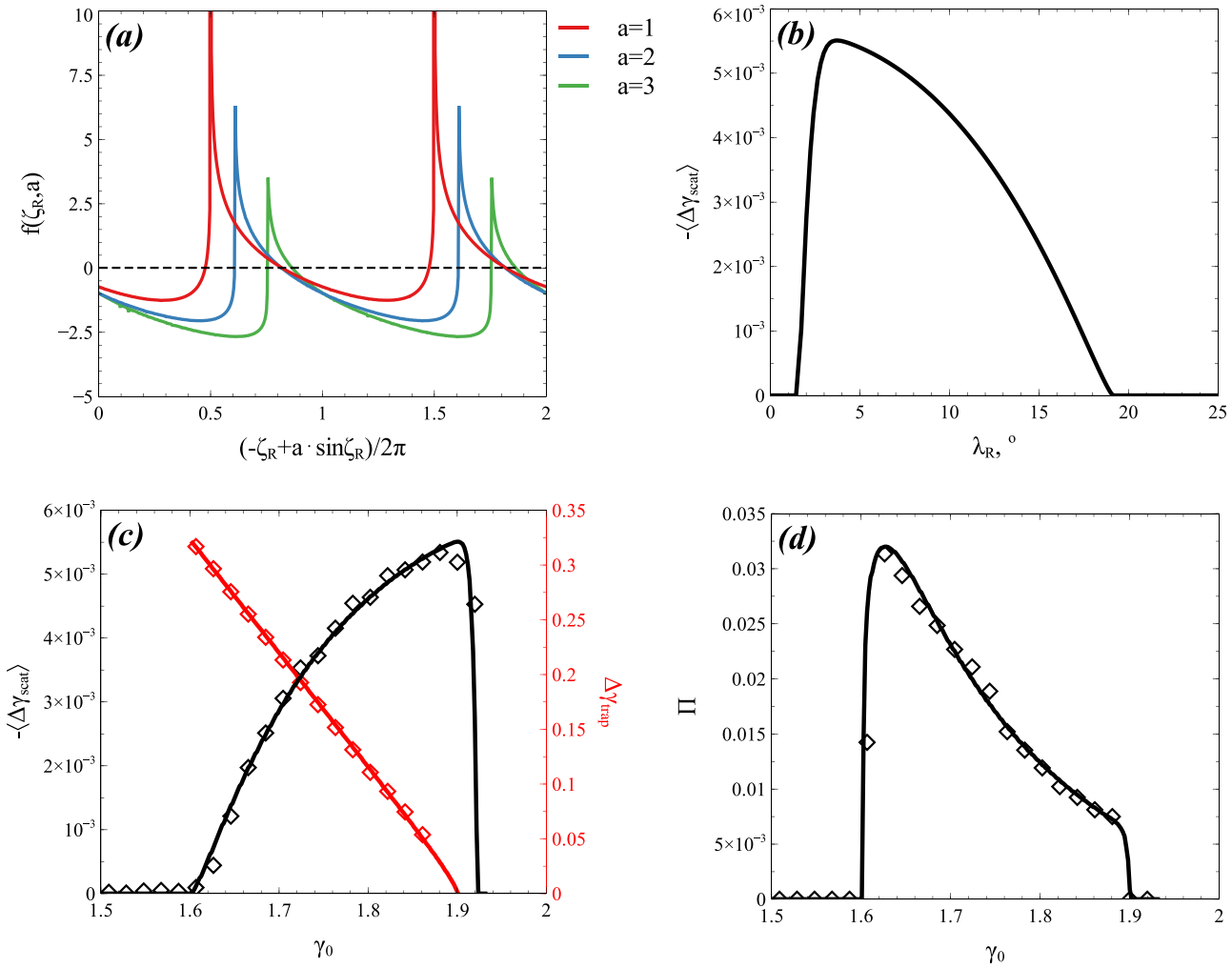

FIG. 2. Main parameters of the resonant system: (a) function $f(\zeta_R, a)$; (b) function $\langle\Delta\gamma_{scat}(\lambda_R)\rangle$, (c) function $\langle\Delta\gamma_{scat}(\gamma_0)\rangle$; (d) probability of trapping $\Pi(\gamma_0)$. Symbols show the results of numerical simulations ($h/m_ec^2 = 1.454$ corresponds to, e.g., $\alpha_0 = 45^\circ$ of the equatorial pitch-angle for 300 keV electron energy; see details of model parameters in the caption of Fig. 1).

the analytical expression (7) in Fig. 2(c): to evaluate $\Delta\gamma_{scat}$ numerically, for several γ_0 we run 10^4 trajectories for Hamiltonian (1) for fixed h and different γ_0 (the time of integration of each trajectory includes only one resonant interaction) and then average energy changes.

In contrast to scattering, particle trapping is a non-local process. The energy change due to trapping significantly exceeds $\Delta\gamma_{scat}$ and can be comparable with the initial particle energy. Particles can be trapped if the probability of trapping Π is positive.[14,63] For system (5), this probability is defined by the relation[22]

$$\Pi = -\frac{m_ec^2}{\omega}\frac{d\Delta\gamma_{scat}}{dI} = -\frac{m_ec^2}{\omega}\{\Delta\gamma_{scat}, I_R\}, \qquad (10)$$

where $\{\cdot,\cdot\}$ is the Poisson bracket with respect to the variables s and P. The value Π depends on the initial energy γ_0 and I_x in terms of their combination $h = -\omega I_{x0} + m_ec^2\gamma_0$. If Eq. (10) gives a negative value, Π should be set to be zero and there are no trapped particles.

Equation (10) determines the relative number of resonant particles that get trapped during a single resonant interaction. Analogous equations have been verified using the test particle calculations for several specific Hamiltonians in Refs. 17, 22, and 91. Note that due to conservation of h, the change of I is equal to the change of $\gamma m_ec^2/\omega$, and thus, Eq. (10) can be written as $\Pi = -d\Delta\gamma_{scat}/d\gamma$, i.e., the derivative of the profile $\Delta\gamma_{scat}(\gamma)$ from Fig. 2(c) should give the $\Pi(\gamma)$ profile (for fixed h). Figure 2(d) shows this $\Pi(\gamma)$ and the corresponding numerical verifications (each numerical point shows the relative amount of 10^4 particles that have been trapped during the first resonant interaction).

Being trapped at some resonant value s_R defined by Eq. (8), particles should escape at s_{detrap} with an energy gain $\Delta\gamma_{trap} = \gamma_R(s_{detrap}) - \gamma_0$. This detrapping coordinate can be calculated using the conservation of the adiabatic invariant $(2\pi)^{-1}\oint P_\zeta d\zeta$ for trapped particles (see details in, e.g., Refs. 17 and 91). Formally speaking, s_{detrap}

is the solution of equation $\Delta\gamma_{scat}(s_{detrap}) = \Delta\gamma_{scat}(s_R)$, i.e., the function (7) should have the same value at the trapping and detrapping positions.[22,94]

To summarize, for a given $h = -\omega I_{x0} + \gamma_0 m_e c^2$, the resonant system (1) can be reduced to a 1D system that is described by the profile of energy change due to scattering $\Delta\gamma_{scat}(\gamma)$, probability of trapping $\Pi = \max(0, -d\Delta\gamma_{scat}/d\gamma)$, and energy change due to trapping $\Delta\gamma_{trap}(\gamma)$. These three functions allow us to construct a map describing the system evolution on a time interval including many resonant interactions.

III. MAPPING TECHNIQUE

Let us discuss the meaning of the probability of trapping, Π. Each trajectory far from the resonance is characterized by initial energy γ, magnetic moment I_x, coordinates in the $(s, p_\parallel)$ plane, and phase ζ which coincides with φ. Knowing these values, we can determine if particles will be trapped or scattered during the first resonant interaction. However, particle phase ζ changes with time much faster than particle $s, p_\parallel$ coordinates ($\dot\zeta \sim \Omega_{ce}$ is the largest frequency in the system). Even a small initial variation of ζ can result in a crucial change of the particle's fate: trapped particles may become scattered and vice versa. Accordingly, instead of tracing individual trajectories with given ζ, it is more suitable to adopt a probabilistic approach and to consider the relative amount of trapped particle trajectories, equal to Π (see Refs. 60 and 72).

Will a particle be trapped or scattered depends on the ζ value at the resonance, ζ_R, but instead of ζ it is more convenient to use the normalized resonant energy $\xi = (a\sin\zeta_R - \zeta_R)/2\pi - (a\sin\zeta_+ - \zeta_+)/2\pi$ [where $\zeta_R \in [\zeta_+ - 2\pi, \zeta_-]$, see Fig. 1(b)], which is distributed uniformly (see numerical tests of ξ distributions in, e.g., Refs. 19 and 37); its values belong to the interval $[0, 1]$. Within this interval, the measure of the sub-range corresponding to trapping equals Π, and this sub-range is $0 \le \xi \le \Pi$. As the particle energy does not change between two successive resonant interactions, we can write a map of the $\gamma \to \bar\gamma$ transition during a single resonance interaction,

$$\bar\gamma = \gamma + \begin{cases} \Delta\gamma_{trap}(\gamma), & \xi \in [0, \Pi), \\ \Delta\gamma_{scat}(\gamma), & \xi \in (\Pi, 1], \end{cases}$$
$$\Pi = -d\Delta\gamma_{scat}/d\gamma. \tag{11}$$

The map (11) should be supplemented with a map for value ξ, which is related to ζ change (gain) between two resonances through the equation [see Eq. (A17) in Appendix],

$$\bar\xi = \xi - \Delta\zeta/2\pi \mod 1. \tag{12}$$

The rate of ζ change is defined by the Hamiltonian system (2) (note that $\zeta = \varphi$), but it is more convenient to use notations of the Hamiltonian system (1),

$$\dot\zeta = -\omega + \frac{\Omega_{ce}(s)}{\gamma} + k(s)\frac{p_\parallel}{m_e\gamma},$$
$$p_\parallel = m_e c\sqrt{\gamma^2 - 1 - \frac{2I_x\Omega_{ce}(s)}{m_e c^2}}. \tag{13}$$

Integrating Eq. (13) over the time interval between two resonances (in the system under consideration this time is equal to the bounce period τ_b), we obtain

$$\Delta\zeta = \omega\tau_b\left(\frac{\varpi}{\gamma} - 1\right),$$
$$\tau_b = \frac{4}{c}\int_0^{s_{\max}}\left(\gamma^2 - 1 - \frac{2I_x\Omega_{ce}(s)}{m_e c^2}\right)^{-1/2} ds,$$
$$\varpi = \frac{\int_0^{s_{\max}}\Omega_{ce}(s)\left(\gamma^2 - 1 - \frac{2I_x\Omega_{ce}(s)}{m_e c^2}\right)^{-1/2} ds}{\int_0^{s_{\max}}\omega\left(\gamma^2 - 1 - \frac{2I_x\Omega_{ce}(s)}{m_e c^2}\right)^{-1/2} ds}, \tag{14}$$

where τ_b and ϖ depend on energy γ and I_x or, at h fixed, these functions depend only on γ (see Fig. 3). Note that the integral $\gamma^{-1}\oint k(s)p_\parallel dt = \oint k(s)ds$ is equal to zero.

Combining Eqs. (14) and (11), we obtain the map for this resonant system in the (γ, ξ) plane:

$$\bar\xi = \xi - \omega\tau_b(\varpi\gamma^{-1} - 1)/2\pi, \quad \Pi = -d\Delta\gamma_{scat}/d\gamma,$$
$$\bar\gamma = \gamma + \begin{cases} \Delta\gamma_{trap}(\gamma), & \bar\xi \in [0, \Pi), \\ \Delta\gamma_{scat}(\gamma), & \bar\xi \in (\Pi, 1]. \end{cases} \tag{15}$$

This map describes variation of particle energy and phase. Figure 4(a) shows a typical trajectory obtained from 200 iterations for map (15): the particle loses energy due to scattering and sometimes (when the phase appears to be within the short range $[0, \Pi)$) gains energy due to trapping. After a sufficiently large number of iterations, the particle trajectory fills the entire (ζ, γ) plane (within the range of the resonant energies for which $\Delta\gamma_{scat} \neq 0$), as shown in Fig. 4(b). This property of map (16) requires sufficiently intense waves, i.e., there is a threshold of wave intensity for stochasticity of particle trajectories. This threshold is determined by the relation of wave amplitude U_w and inhomogeneity of the phase gain, $\partial(\bar\xi - \xi)/\partial\gamma$ (see the general form of this relation in Ref. 12).

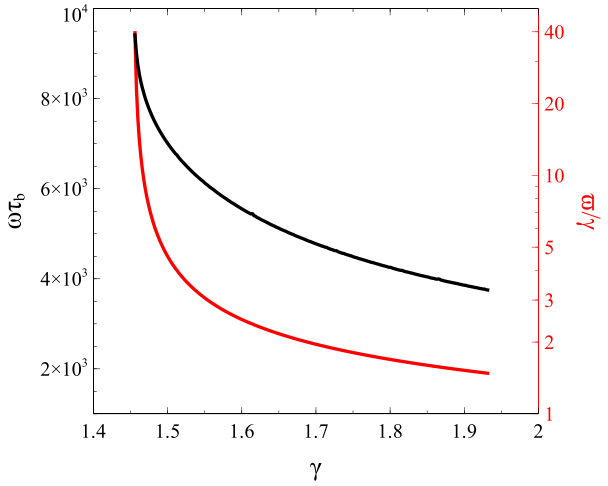

FIG. 3. Functions $\omega\tau_b(\gamma)$, $\varpi(\gamma)$ for a fixed value of h ($h/m_e c^2 = 1.454$ corresponding, e.g., to an equatorial pitch-angle $\alpha_0 = 45^\circ$ for a 300 keV electron; see details of model parameters in the caption of Fig. 1).

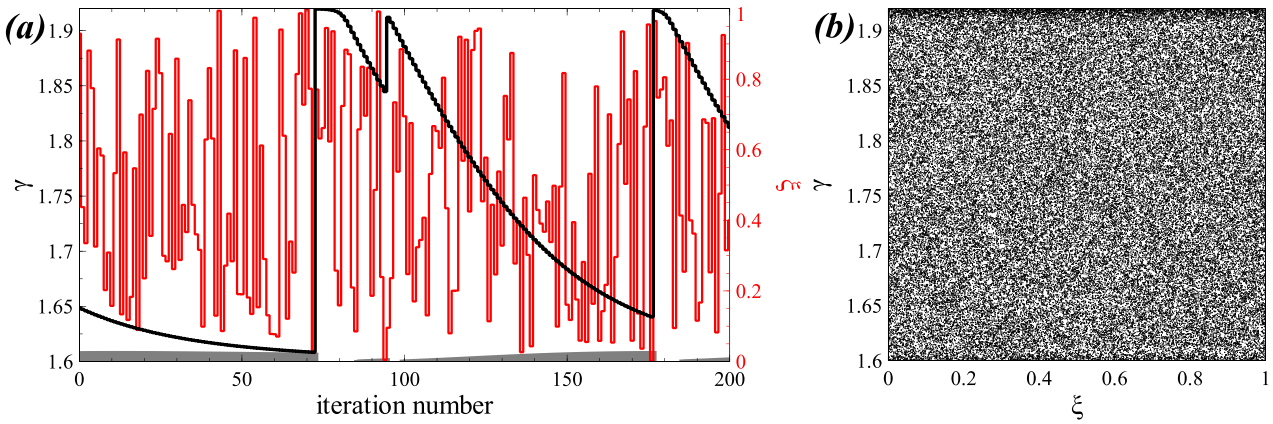

FIG. 4. (a) Particle trajectory for map (15): γ and ξ as functions of iteration number, gray color shows the capture probability Π. (b) Particle trajectory in (ξ, γ) plane for 10^5 iterations. ($h/m_e c^2 = 1.454$ corresponds to, e.g., $\alpha_0 = 45^\circ$ of the equatorial pitch-angle for 300 keV electron energy; see details of model parameters in the caption of Fig. 1).

The spreading of a single trajectory means that any initial distribution of energy should tend toward a uniform distribution (note that we are speaking of energies for a fixed h, i.e., the energy distribution along the resonant curve[56,78]). A similar result has been obtained through numerical simulations and solutions[59] of the kinetic equation[15] describing the long-term dynamics of many trajectories (1). In Sec. IV, to check the derived map (15), we compare the results provided by this map with results of test particle simulations, as well as with results obtained by solving the full kinetic equation.

IV. VERIFICATION OF MAPPING RESULTS

Let us fix h and consider a 1D energy distribution $\Psi(\gamma)$ (note that Ψ is a cut of the 2D energy/pitch-angle distribution). We can represent this distribution as a set of 10^6 individual particles with different initial energies and randomly distributed phases. Then, the trajectory of each particle can be traced numerically using Hamiltonian equations (1) over a time interval including many resonance interactions. This method reproduces the evolution of $\Psi(\gamma)$ driven by the wave-particle resonant interaction. Alternatively, we can trace trajectories and reproduce the evolution of $\Psi(\gamma)$ using the map (15). The third approach is to solve the kinetic equation that describes Ψ evolution due to nonlinear resonant interactions,[15,18]

$$\frac{\partial \Psi}{\partial t} = V\frac{\partial \Psi}{\partial J} + \frac{dV}{dJ}(\Psi^* - \Psi)\Theta(J), \tag{16}$$

where $J(\gamma) = \int^{\gamma} \tau_b(\gamma')d\gamma'$, $V = \Delta\gamma_{scat}/\tau_b$, $\Psi^* = \Psi(\gamma^*)$ with $\gamma^* + \Delta\gamma_{trap}(\gamma^*) = \gamma$, and $\Theta = 0$ for $\Pi = 0$ and $\Theta = 1$ for $\Pi > 0$. Equation (16) can be re-written in a simplified form,

$$\frac{\partial \Psi}{\partial t} = V\frac{\partial \Psi}{\partial \gamma} + \frac{dV}{d\gamma}(\Psi^*\tau_b(\gamma^*)/\tau_b(\gamma) - \Psi)\Theta(\gamma) + \ell, \tag{17}$$

where the term ℓ includes derivatives $\sim\partial\tau_b/\partial\gamma$ and can be omitted for a sufficiently weak $\tau_b(\gamma)$ dependence [see details of $\gamma \to J(\gamma)$ transformation in Refs. 16 and 18].

We consider such three types of solutions of $\Psi(\gamma)$ evolution [test particles, Eq. (16), and map (15)] for two initial distributions Ψ. Figure 5 shows these three solutions for initial power law energy distribution and three moments of time (note that solutions obtained via test particle simulations and Eq. (16) depend on time, whereas the map (15) depends on the iteration number that should be transformed to time using the bounce period $\tau_b(\gamma)$ for each trajectory). All three solutions show a very similar evolution of $\Psi(\gamma)$: the distribution gets flattened within the resonant energy range (where $\Delta\gamma_{scat} \neq 0$) and forms a plateau. This is the effect of a competition between trapping (energy increase) and scattering (energy decrease) that ultimately results in a uniform distribution (note that this uniform distribution is formed along the resonance curves,[56,78] i.e., for $h = \text{const}$). A similar evolution, although more complicated, can be seen in Fig. 6 showing three solutions for an initial $\Psi(\gamma)$ with a local maximum. This maximum starts drifting to lower energies (due to scattering), whereas a new maximum forms at high energies (due to trapping acceleration). Finally, $\Psi(\gamma)$ will be flattened and form a plateau within the resonant energy range. Such an evolution of $\Psi(\gamma)$ has been predicted and described [considering solutions of Eq. (16)] in Refs. 11 and 59.

The flattening of the $\Psi(\gamma)$ distribution for fixed h corresponds to decay of gradients of the 2D (energy, pitch-angle) electron distribution along the resonance curve. These curves are defined as solutions of combined equations of resonant condition and energy conservation in the wave reference frame.[56,78] For a narrow wave spectrum, the quasi-linear diffusion also reduces gradients along these curves in the 2D space of (energy, pitch-angle), i.e., results shown in Figs. 5 and 6 are in agreement with the theory of the quasi-linear diffusion. However, nonlinear wave-particle interaction reduces gradients along resonance curves much faster than the quasi-linear diffusion does (see the discussion in Ref. 11).

V. DISCUSSION

In this study, we have developed a map describing the dynamics of systems with nonlinear resonant wave-particle interactions. For illustration, we used wave and background plasma parameters typical of the Earth inner magnetosphere, where relativistic electrons resonate with high amplitude whistler-mode waves. This system is well investigated in the regime of low wave amplitudes where quasi-linear diffusion equations are applicable,[56,74,84] but so far there is no method allowing to model the long-term evolution of this system in the presence of nonlinear resonant effects. One of the most widespread

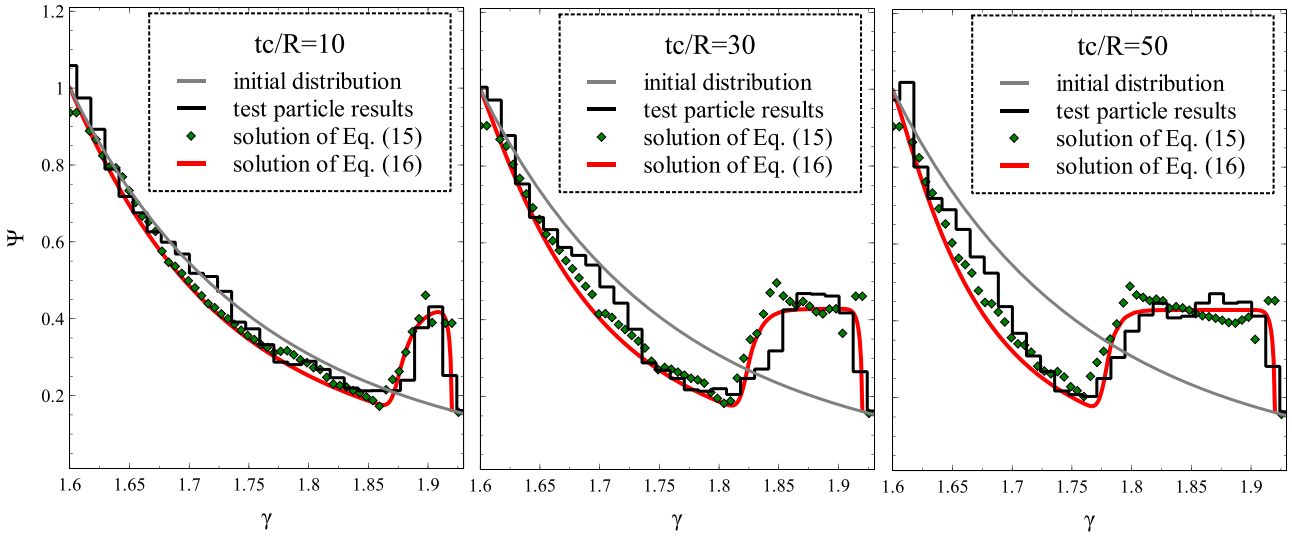

FIG. 5. Evolution of distribution $\Psi(\gamma)$ for $h/m_e c^2 = 1.454$ (this value of h corresponds to, e.g., equatorial pitch-angle $\alpha_0 = 45^\circ$ for 300 keV electron energy; see details of the model parameters in the caption to Fig. 1): black color shows results of test particle simulations (10^6 trajectories), red color shows solutions of Eq. (16), and green color shows results of mapping (15). The initial distribution $\Psi(\gamma)$ is shown in all panels with gray curves. Time is normalized on R/c (a scale of the quarter of the bounce period) with $R = 4.5$ Earth radii.

techniques, test particle simulation,[5,25,28,29,41,58,67] provides a lot of important information about electron acceleration and scattering rates, but such simulations are limited to quite short time intervals. This limitation mostly comes from the need to integrate the entire (bounce) particle trajectory even if energy and magnetic moment only change at the locations of wave-particle resonances. Therefore, a natural solution consists of considering only resonance-induced changes of particle energy and pitch-angle, like in the quasi-linear diffusion approach. The generalization of the diffusion equation with inclusion of terms related to nonlinear wave-particle interaction results in Eq. (16) or similar types of kinetic equations.[15,18,75] However, this kinetic equation still relies on the assumption of a uniform distribution of resonant phases (i.e., it excludes effects related to phase correlation at multiple passages through the resonance) and it cannot be easily generalized for systems with multiple waves. These two problems can be resolved using the map approach that includes resonant phase dynamics while

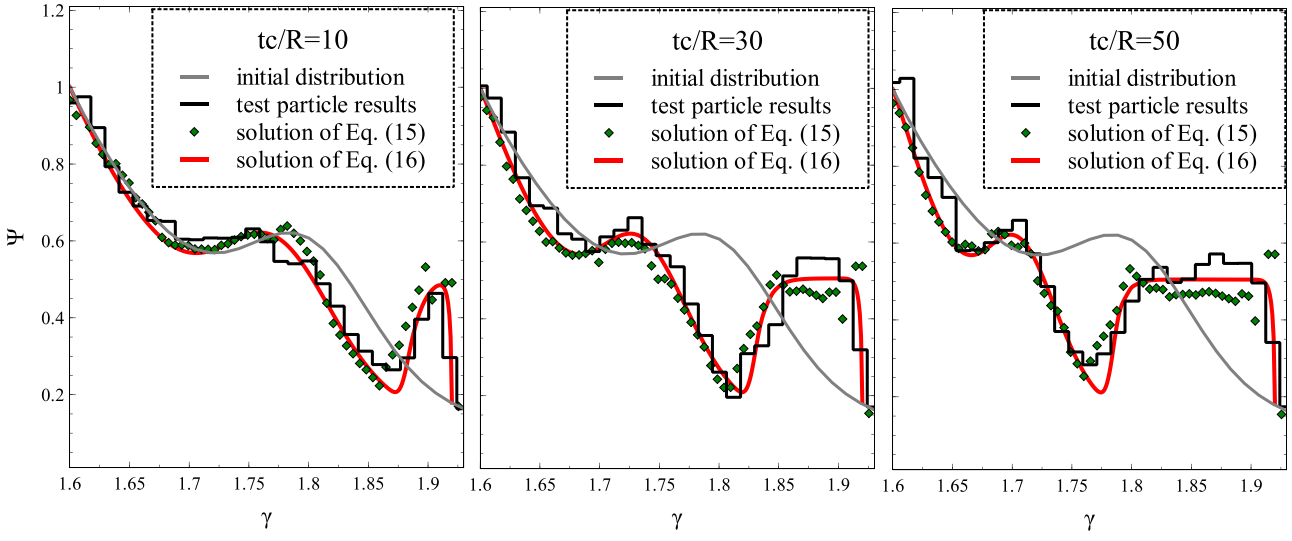

FIG. 6. Evolution of the distribution $\Psi(\gamma)$ for $h/m_e c^2 = 1.454$ (this value of h corresponds to, e.g., equatorial pitch-angle $\alpha_0 = 45^\circ$ for 300 keV electron energy; see details of the model parameters in the caption of Fig. 1): black color shows results of test particle simulations (10^6 trajectories), red color shows solutions of Eq. (16), and green color shows results of mapping (15). The initial distribution $\Psi(\gamma)$ is shown in all panels with gray curves. Time is normalized to R/c (the quarter of the bounce period) with $R = 4.5$ Earth radii.

also allowing the inclusion of many resonances. Let us consider these two issues in more detail.

Assuming a uniform distribution of resonant phases corresponds to the assumption that two successive resonances are not correlated, i.e., that electron energy jumps $\Delta\gamma$ (due to trapping or scattering) can be considered as independent over a long run. This important property of the resonant system usually results from the dependence of the phase gain $\Delta\zeta$ on energy γ [see Eq. (15)]. This gain is usually large $\Delta\zeta \sim \omega\tau_b \gg 1$ (since the whistler-mode wave period is much smaller than the electron bounce period along magnetic field lines) and, thus, even a small change of energy $\Delta\gamma$ due to resonant interaction should result in a significant change of $\Delta\zeta$: $\delta(\Delta\zeta) \sim (\partial\Delta\zeta/\partial\gamma)\Delta\gamma$, justifying the assumption of randomly distributed phases. However, resonances can be correlated (and the distribution of resonant phases can be non-uniform, see Ref. 12) for systems with small $\partial\Delta\zeta/\partial\gamma$. Such a situation can hardly appear in the Earth radiation belts, but it is more realistic for resonant electron interaction with strong electrostatic waves and solitons around the bow shock.[95] This corresponds to Landau resonant interaction without the term ϖ/γ in Eq. (15) and with the time interval between resonances $\sim\tau_b$ weakly depending on energy. Therefore, the proposed map technique may be useful for investigations of nonlinear wave-particle interactions in such systems, where the assumption of a uniform distribution of resonant phases is not applicable.

The map (15) has been constructed for a system with a single wave (single resonance). In this system, the condition $h = \text{const}$ reduces the initially 2D space [energy/pitch-angle or (γ, I_x)] to 1D space. However, unlike kinetic equation (16), this map can be generalized to many resonances resulting in particle motion in the (γ, I_x) space. Indeed, the map describes change of the resonant phase ζ between two resonances and energy change on the resonance. The ζ change can be modified by replacing the integration over the entire bounce period with the integration between two resonances in Eq. (14), whereas the energy change can be replaced with energy and I_x changes. This generalization looks much simpler to achieve than the corresponding generalization of the kinetic equation (16).

Figure 4 shows that after many iterations the particle trajectory fills the entire available space in the (ζ, γ) space. For ensembles including many trajectories, the final state of the distribution function will be a uniform distribution where phase space density Ψ should have the same value for all energies. This is the final state for both quasi-linear diffusion, that tends to reduce gradients of Ψ along the resonance curve, and nonlinear wave-particle interaction described by Eq. (16), which has only one stationary solution $\Psi = \text{const}$ (see Ref. 11). Therefore, the map (15) describes distribution flattening, $\partial\Psi/\partial\gamma \to 0$, and allows estimating a typical timescale of this flattening. For example, Fig. 7 shows the evolution of the dispersion $D = \sqrt{\langle\gamma^2\rangle - \langle\gamma\rangle^2}$ of distribution Ψ for four different initial Ψ (shown in the inserted panel). The dynamics of Ψ is described by 10^5 trajectories of map (15), and D is normalized to the dispersion of the uniform distribution for the same γ range (i.e., $D/D_0 \approx 1$ means $\Psi \approx$ const; initial phases of trajectories are random and distributed uniformly). As the map (15) describes discrete changes of energy with time, the beginning of the D evolution consists of step-like jumps (note that we transformed the iteration number to time for each trajectory to plot D vs time). Each jump corresponds to one map iteration. Jumps occur at approximately

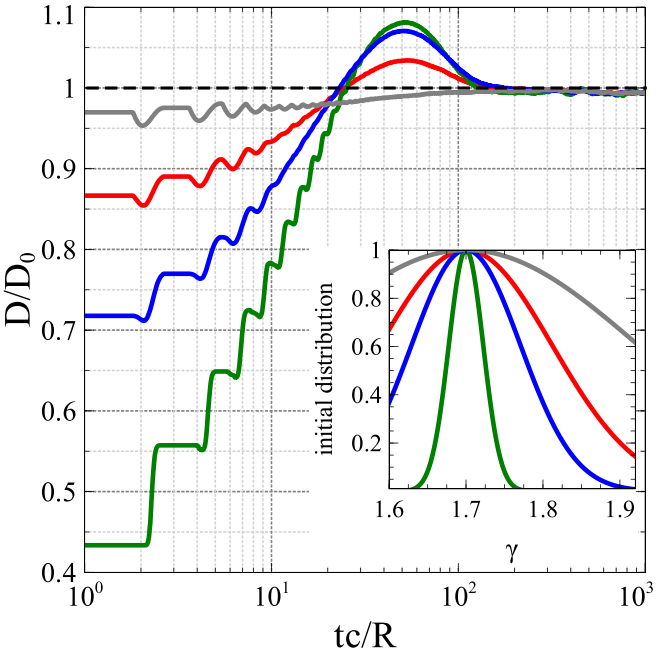

FIG. 7. Evolution of dispersion $D = \sqrt{\langle\gamma^2\rangle - \langle\gamma\rangle^2}$ for four distributions $\Psi(\gamma)$ and $h/m_e c^2 = 1.454$ (this value of h corresponds to, e.g., 45° of the equatorial pitch-angle for 300 keV electron energy; see details of model parameters in the caption of Fig. 1). Dispersions are normalized to the dispersion D_0 of the uniform distribution $\Psi = \text{const}$.

the same time for all trajectories (the time between two jumps weakly depends on energy, $\tau_b(\gamma)$, and does not depend on phase ξ); thus, step-like jumps in Fig. 7 correlate well for different initial distributions. Independently of the initial distribution, $D/D_0 \approx 1$ after $\approx 100\tau_b$, and this timescale is much shorter than typical quasi-linear time scales[53,85] (note for initially narrow distributions, the nonlinear wave-particle interaction includes formation of two maxima on a certain time interval, see Fig. 6, and such two-maximum distributions can have $D/D_0 > 1$).

There is an important point to note about map Eq. (15): this map has been constructed using Hamiltonian equations of electron interaction with a coherent sinusoidal wave. More realistic whistler-mode waves are propagating in the form of localized wave packets with significant amplitude modulation[106] and variation of phase coherence.[3,89] These effects can essentially alter the wave-particle interaction, mostly reducing the efficiency of nonlinear resonant acceleration and scattering.[32,79,80] The wave amplitude modulation may be included in theoretical description of nonlinear wave-particle interaction,[13,59] whereas effects of phase coherence are yet to be investigated theoretically. Therefore, the presented map technique requires further modifications to model realistic whistler-mode characteristics.

To conclude, in this paper, we have considered nonlinear resonances between relativistic electrons and intense whistler-mode waves. We have demonstrated that the long-term dynamics of the electron distribution can be described by a map taking into account the important interdependence between the probability of trapping Π and energy change due to scattering $\Delta\gamma_{scat}$: $\Pi = -d\Delta\gamma_{scat}/d\gamma$. This map is

different from the classical Chirikov map[27] and allows describing both effects of phase trapping and nonlinear scattering. The proposed mapping technique can be useful for the description of charged particle acceleration in various space plasma systems including the Earth radiation belts and the Earth bow shock.

ACKNOWLEDGMENTS

The authors are grateful to Dr. D. Mourenas for useful discussion. This work was supported by the Russian Scientific Foundation, Project No. 19-12-00313. A.V.A. also acknowledges NSF Project No. 1914670.

APPENDIX: PHASE VARIATION

In this Appendix, we derive formula (12), which expresses variation of variable ξ between two resonance crossings via gain of phase ζ between these crossings. We consider a quite general form of Hamiltonian. Results of our derivation are directly applicable to the particular system considered in the main text. This derivation is somewhat similar to the derivation provided in Ref. 61 for change of phase between separatrix crossings. Important to notice that, following the system description in the main text, we consider one resonance crossing per one period of slow motion, i.e., the two resonance crossings are separated in time by one slow period.

Let us consider a general Hamiltonian as the sum of an unperturbed part $H_0(I,p,q)$ and a small perturbation $\varepsilon H_1(I,\zeta,p,q)$ (with $\varepsilon \ll 1$; note in the main text $\varepsilon \sim B_w/B_0$) where $(q,\varepsilon^{-1}p)$, (ζ,I) are pairs of conjugate variables (hence (ζ,I) are fast variables, (q,p) are slow variables), and H_1 is periodic in ζ. Momentum I is an adiabatic invariant: $\dot{I} = -\varepsilon\partial H_1/\partial\zeta$, and I is constant in the averaged over ζ system. There is no explicit dependence on time, and thus, $H = h = \text{const}$. The resonance condition is determined by the equation $\partial H_0/\partial I = 0$. Solving this equation for I gives the equation $I = I_R(p,q)$ of the resonance surface. Denote $\Lambda(p,q) = H_0(I_R(p,q),p,q)$. The Hamiltonian can be expanded around the resonance surface similarly to Eq. (5). We assume that the phase portrait of the expanded Hamiltonian looks like the one shown in Fig. 8.

We introduce the improved adiabatic invariant J with the variable transformation $(I,\zeta,p,q)\mapsto(J,\theta,P,Q)$ such that the new Hamiltonian is $H = H_0(J,P,Q) + \varepsilon\bar{H}_1(J,P,Q)$ where $\bar{H}_1$ is the average of H_1 over ζ (in the leading approximation).

Far from the resonance, θ changes with the frequency,

$$\dot{\theta} = \frac{\partial H_0}{\partial J} + \varepsilon\frac{\partial \bar{H}_1}{\partial J} \tag{A1}$$

with $J = \text{const}$, and

$$\dot{Q} = \varepsilon\frac{\partial H_0}{\partial P} + \varepsilon^2\frac{\partial \bar{H}_1}{\partial P}, \quad \dot{P} = -\varepsilon\frac{\partial H_0}{\partial Q} - \varepsilon^2\frac{\partial \bar{H}_1}{\partial Q}. \tag{A2}$$

We introduce $\omega_0(J,P,Q) = \partial H_0/\partial J$, $\omega_1(J,P,Q) = \partial\bar{H}_1/\partial J$, and consider large number $N \gg 1$ of rounds of ζ from $t = t_0$ (when the phase point is far from the resonance and moves toward the resonance) to $t = t_N$; the last round is sufficiently far from the resonance and $\theta \approx \zeta$ in the leading approximation. The last round ends at $\zeta = \zeta_c \bmod 2\pi$ (see Fig. 8 for the definition of ζ_c). Then,

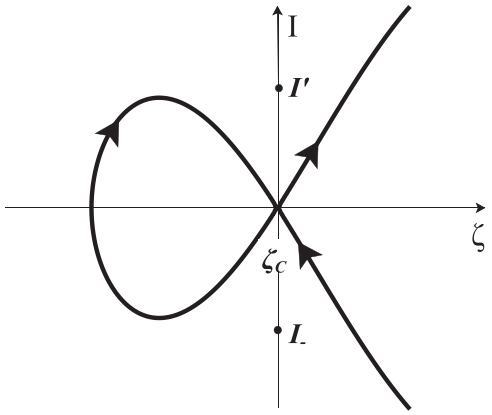

FIG. 8. Schematic of the phase portrait.

$$\zeta_{cN} = \zeta_0 + \int_{t_0}^{t_N}(\omega_0 + \varepsilon\omega_1)dt \mod 2\pi, \tag{A3}$$

where ζ_{cN} is ζ_c value at $t = t_N$. We introduce t_* as the time of crossing the resonance, i.e., $\omega_0(J,P,Q)|_{t=t_*} = 0$, and rewrite Eq. (A3) as

$$\zeta_{cN} = \zeta_0 + \int_{t_0}^{t_*}(\omega_0 + \varepsilon\omega_1)dt - \int_{t_N}^{t_*}(\omega_0 + \varepsilon\omega_1)dt \mod 2\pi. \tag{A4}$$

Because $t_* - t_N \ll 1/\varepsilon$, we can use $\dot{Q} = \varepsilon\partial H_0/\partial P$, $\dot{P} = -\varepsilon\partial H_0/\partial P$, and $Q \approx q$, $P \approx p$ in the last integral in Eq. (A4). We also assume that $\zeta_{cN} \approx \zeta_{c*} = \zeta_c|_{t=t_*}$. To describe system dynamics for $t \in [t_N, t_*]$, we use the expansion of the Hamiltonian around the resonance: $H = \Lambda + F$ and

$$F = \frac{1}{2}g(I - I_R)^2 + \varepsilon H_1, \quad g = \left.\frac{\partial^2 H_0}{\partial I^2}\right|_{I=I_R} \approx \text{const}. \tag{A5}$$

The Hamiltonian in new variables (J,θ,P,Q) can be expanded as

$$H = \Lambda + \frac{1}{2}g(J - I_R)^2 + \varepsilon\bar{H}_1. \tag{A6}$$

We introduce $e = g(J - I_R)^2/2$ and write

$$\dot{e} = \varepsilon g(J - I_R)r, \quad r = -\{I_R, \Lambda\} \approx \text{const},$$
$$\omega_0 = \frac{\partial H}{\partial J} = g(J - I_R). \tag{A7}$$

Using $dt = de/(de/dt)$, we rewrite the integral

$$\int_{t_N}^{t_*}(\omega_0 + \varepsilon\omega_1)dt \approx \frac{1}{\varepsilon}\int_{e_N}^{0}\frac{\omega_0 de}{g(J - I_R)r} = \frac{1}{\varepsilon}\int_{e_N}^{0}\frac{de}{r} = -\frac{e_N}{\varepsilon r}, \tag{A8}$$

where e_N is the value e along the trajectory at $t = t_N$, and we omit $\varepsilon\omega_1$ because $t_* - t_N \ll 1/\varepsilon$. Using $e + \varepsilon\bar{H}_1 = F$, we write

$$e_N = F_N - \varepsilon\bar{H}_1 \approx F_N - \varepsilon\bar{H}_{1*}, \tag{A9}$$

where F_N is the value F along the trajectory at $t = t_N$, and $\bar{H}_{1*}$ is the resonant value of $\bar{H}_1$. Substituting Eqs. (A8) and (A9) to Eq. (A4), we obtain

$$\zeta_{c*} = \zeta_0 + \int_{t_0}^{t_*} (\omega_0 + \varepsilon\omega_1)dt + \frac{F_N - \varepsilon\bar{H}_{1*}}{\varepsilon r} \mod 2\pi \tag{A10}$$

or

$$\frac{F_N}{2\pi\varepsilon r} = \frac{\bar{H}_{1*}}{2\pi r} - \frac{1}{2\pi}\left(\zeta_0 - \zeta_{c*} + \int_{t_0}^{t_*} (\omega_0 + \varepsilon\omega_1)dt\right) \mod 1. \tag{A11}$$

We define F_{last} as the value of F along the trajectory at the last crossing of the line $\zeta = \zeta_c$ before crossing the resonance. Thus, $F_{last} = F_N \bmod 2\pi\varepsilon r$, because the change of F for one round of ζ equals $2\pi\varepsilon r$. We introduce $\xi = (F_{last} - \varepsilon H_{1c*})/(2\pi\varepsilon r)$, where H_{1c*} is the value of H_1 at $\zeta = \zeta_c$, $t = t_*$ and write

$$\xi = \mathrm{Frac}\left(\frac{\bar{H}_{1*} - H_{1c*}}{2\pi r} - \frac{\zeta_0 - \zeta_{c*}}{2\pi} - \frac{1}{2\pi\varepsilon}\int_{\tau_0}^{\tau_*} (\omega_0 + \varepsilon\omega_1)d\tau\right). \tag{A12}$$

Here, $\tau = \varepsilon t$, $\tau_* = \varepsilon t_*$. Note that ξ can be written as

$$\xi = \frac{F_{last} - \varepsilon H_{1c*}}{2\pi\varepsilon r} = \frac{F_{last} - \varepsilon r\zeta_{c*} - (\varepsilon H_{1c*} - \varepsilon r\zeta_{c*})}{2\pi\varepsilon r}, \\ = \frac{E_{last} - E_{c*}}{2\pi\varepsilon r}, \tag{A13}$$

where

$$E = \frac{1}{2}g(I - I_R)^2 - \varepsilon r\zeta + \varepsilon H_1, \tag{A14}$$

and E_{c*} is the value of E at $\zeta = \zeta_c$, $t = t_*$, and E_{last} is the value of E at the last crossing of the line $\zeta = \zeta_c$ before crossing the resonance.

Let us use Eq. (A12) to consider two successive resonance crossings (note that there is only one resonant interaction for one period of slow motion, i.e., two successive resonance crossings are separated by one slow period). Far from the resonance, the improved adiabatic invariant J can be considered as a constant. Denote τ_- and τ_+ slow time moments of the resonance crossings ($\tau = \varepsilon t$). Let $\xi_\pm$ be values of the variable ξ corresponding to these two crossings. We are looking for a relation between ξ_+ and ξ_-. Due to periodicity of the slow motion, values of ζ_{c*}, H_{1c*}, $\bar{H}_{1*}$, r are the same at $\tau = \tau_+$ and $\tau = \tau_-$.

We consider value ξ_- for the first of the resonance crossings, and the corresponding value $E = E_{last-}$. At $\tau = \tau_-$, the phase point is on the line $\zeta = \zeta_{c*}$ with $I < I_R$ at the position indicated by the symbol I_- in Fig. 8. We assume that this phase point crosses the resonance without trapping. Thus, at some $\tau = \tau'$ it arrives again to the line $\zeta = \zeta_c = \zeta'_{c*}$ with the value $E = E'$ and $I > I_R$. The phase point position is indicated by the symbol I' in Fig. 8. We denote $\xi' = (E' - E_{c*})/(2\pi\varepsilon r)$. We have $E' \approx E_{last-}$, $\xi' \approx \xi_-$.

At some moment of the slow time $\tau_0 \in (\tau_-, \tau_+)$, the phase point is far from the resonance and has $\zeta = \zeta_0$. Then, Eq. (A12) gives

$$\xi_+ = \mathrm{Frac}\left(\frac{\bar{H}_{1*} - H_{1c*}}{2\pi r} - \frac{\zeta_0 - \zeta_{c*}}{2\pi} - \frac{1}{2\pi\varepsilon}\int_{\tau_0}^{\tau_+} (\omega_0 + \varepsilon\omega_1)d\tau\right). \tag{A15}$$

Similarly, considering the backward motion on the time interval from τ_0 to τ', we get

$$\xi' = \mathrm{Frac}\left(\frac{\bar{H}_{1*} - H_{1c*}}{2\pi r} - \frac{\zeta_0 - \zeta_{c*}}{2\pi} + \frac{1}{2\pi\varepsilon}\int_{\tau'}^{\tau_0} (\omega_0 + \varepsilon\omega_1)d\tau\right). \tag{A16}$$

In this expression, we can replace in the leading approximation ξ' with ξ_- and τ' with τ_- (note that

$$\frac{1}{2\pi\varepsilon}\int_{\tau_-}^{\tau'} (\omega_0 + \varepsilon\omega_1)d\tau$$

is small, because ω_0 vanishes on the resonant surface). Thus, for the value $\Delta\xi = \xi_+ - \xi_-$, we get

$$\Delta\xi = \xi_+ - \xi_- = -\frac{1}{2\pi\varepsilon}\int_{\tau_-}^{\tau_+} (\omega_0 + \varepsilon\omega_1)d\tau \bmod 1, \tag{A17}$$

and this is the phase ζ gain between two resonance crossings (between moments τ_- and τ_+) normalized on 2π and taken with the minus sign. In the main text, $\bar{H}_1 = 0$ and, thus, $\omega_1 = \partial\bar{H}_1/\partial J = 0$.

REFERENCES

[1] O. Agapitov, A. Artemyev, V. Krasnoselskikh, Y. V. Khotyaintsev, D. Mourenas, H. Breuillard, M. Balikhin, and G. Rolland, J. Geophys. Res. **118**, 3407–3420, https://doi.org/10.1002/jgra.50312 (2013).

[2] O. Agapitov, A. Artemyev, D. Mourenas, V. Krasnoselskikh, J. Bonnell, O. Le Contel, C. M. Cully, and V. Angelopoulos, J. Geophys. Res. **119**, 1606–1626, https://doi.org/10.1002/2013JA019223 (2014).

[3] O. Agapitov, V. Krasnoselskikh, T. Dudok de Wit, Y. Khotyaintsev, J. S. Pickett, O. Santolík, and G. Rolland, J. Geophys. Res. **116**, 9222, https://doi.org/ (2011).

[4] O. V. Agapitov, A. V. Artemyev, D. Mourenas, F. S. Mozer, and V. Krasnoselskikh, Geophys. Res. Lett. **42**, 3715, https://doi.org/10.1002/2015GL064145 (2015).

[5] O. V. Agapitov, D. Mourenas, A. V. Artemyev, and F. S. Mozer, Geophys. Res. Lett. **43**, 11,112–11,120, https://doi.org/10.1002/2016GL071250 (2016).

[6] J. M. Albert, Phys. Fluids B **5**, 2744–2750 (1993).

[7] J. M. Albert, Geophys. Res. Lett. **29**, 1275, https://doi.org/10.1029/2001GL013941 (2002).

[8] J. M. Albert, X. Tao, and J. Bortnik, "Aspects of nonlinear wave-particle interactions," in *Dynamics of the Earth's Radiation Belts and Inner Magnetosphere*, edited by D. Summers, I. U. Mann, D. N. Baker, and M. Schulz (American Geophysical Union, 2013).

[9] X. An, B. Van Compernolle, J. Bortnik, R. M. Thorne, L. Chen, and W. Li, Geophys. Res. Lett. **43**, 2413–2421, https://doi.org/10.1002/2015GL067126 (2016).

[10] A. Artemyev, O. Agapitov, D. Mourenas, V. Krasnoselskikh, V. Shastun, and F. Mozer, Space Sci. Rev. **200**, 261–355 (2016).

[11] A. Artemyev, A. Neishtadt, and A. Vasiliev, Physica D **393**, 1–8 (2019); arXiv:1809.03743.

[12] A. Artemyev, A. Neishtadt, and A. Vasiliev, Regular Chaotic Dyn. **25**, 2–10 (2020).

[13]A. V. Artemyev, D. Mourenas, O. V. Agapitov, D. L. Vainchtein, F. S. Mozer, and V. V. Krasnoselskikh, Phys. Plasmas **22**, 082901 (2015).
[14]A. V. Artemyev, A. I. Neishtadt, D. L. Vainchtein, A. A. Vasiliev, I. Y. Vasko, and L. M. Zelenyi, Commun. Nonlinear Sci. Numer. Simul. **65**, 111–160 (2018).
[15]A. V. Artemyev, A. I. Neishtadt, A. A. Vasiliev, and D. Mourenas, Phys. Plasmas **23**, 090701 (2016).
[16]A. V. Artemyev, A. I. Neishtadt, A. A. Vasiliev, and D. Mourenas, arXiv:1710.04489 (2017).
[17]A. V. Artemyev, A. I. Neishtadt, A. A. Vasiliev, and D. Mourenas, Phys. Rev. E **95**, 023204 (2017).
[18]A. V. Artemyev, A. I. Neishtadt, A. A. Vasiliev, and D. Mourenas, J. Plasma Phys. **84**, 905840206 (2018).
[19]A. V. Artemyev, A. I. Neishtadt, and L. M. Zelenyi, Chaos **21**, 043120 (2011).
[20]A. V. Artemyev, A. A. Vasiliev, D. Mourenas, O. Agapitov, V. Krasnoselskikh, D. Boscher, and G. Rolland, Geophys. Res. Lett. **41**, 5727–5733, https://doi.org/10.1002/2014GL061380 (2014).
[21]A. V. Artemyev, A. A. Vasiliev, D. Mourenas, O. V. Agapitov, and V. V. Krasnoselskikh, Phys. Plasmas **21**, 102903 (2014).
[22]A. V. Artemyev, A. A. Vasiliev, D. Mourenas, A. I. Neishtadt, O. V. Agapitov, and V. Krasnoselskikh, Phys. Plasmas **22**, 112903 (2015).
[23]T. F. Bell, J. Geophys. Res. **89**, 905–918, https://doi.org/10.1029/JA089iA02p00905 (1984).
[24]S. Benkadda, A. Sen, and D. R. Shklyar, Chaos **6**, 451–460 (1996).
[25]J. Bortnik, R. M. Thorne, and U. S. Inan, Geophys. Res. Lett. **35**, 21102, https://doi.org/10.1029/2008GL035500 (2008).
[26]C. Cattell, J. R. Wygant, K. Goetz, K. Kersten, P. J. Kellogg, T. von Rosenvinge, S. D. Bale, I. Roth, M. Temerin, M. K. Hudson, R. A. Mewaldt, M. Wiedenbeck, M. Maksimovic, R. Ergun, M. Acuna, and C. T. Russell, Geophys. Res. Lett. **35**, 1105, https://doi.org/10.1029/2007GL032009 (2008).
[27]B. V. Chirikov, Phys. Rep. **52**, 263–379 (1979).
[28]A. G. Demekhov, V. Y. Trakhtengerts, M. Rycroft, and D. Nunn, Geomagn. Aeron. **49**, 24–29, https://doi.org/10.1134/S0016793209010034 (2009).
[29]A. G. Demekhov, V. Y. Trakhtengerts, M. J. Rycroft, and D. Nunn, Geomagn. Aeron. **46**, 711–716, https://doi.org/10.1134/S0016793206060053 (2006).
[30]X. Fu, M. M. Cowee, R. H. Friedel, H. O. Funsten, S. P. Gary, G. B. Hospodarsky, C. Kletzing, W. Kurth, B. A. Larsen, K. Liu, E. A. MacDonald, K. Min, G. D. Reeves, R. M. Skoug, and D. Winske, J. Geophys. Res **119**, 8288–8298, https://doi.org/10.1002/2014JA020364 (2014).
[31]N. Furuya, Y. Omura, and D. Summers, J. Geophys. Res. **113**, 4224, https://doi.org/10.1029/2007JA012478 (2008).
[32]L. Gan, W. Li, Q. Ma, J. M. Albert, A. V. Artemyev, and J. Bortnik, Geophys. Res. Lett. **47**, e2019GL085987, https://doi.org/10.1029/2019GL085987 (2020).
[33]S. P. Gary and J. Wang, J. Geophys. Res. **101**, 10749–10754, https://doi.org/10.1029/96JA00323 (1996).
[34]Y. K. Hsieh, Y. Kubota, and Y. Omura, J. Geophys. Res. **125**, e2019JA027465, https://doi.org/10.1029/2019JA027465 (2020).
[35]Y. K. Hsieh and Y. Omura, J. Geophys. Res. **122**, 675–694, https://doi.org/10.1002/2016JA023255 (2017).
[36]Y. K. Hsieh and Y. Omura, Radio Sci. **52**, 1268–1281, https://doi.org/10.1002/2017RS006245 (2017).
[37]A. P. Itin, A. I. Neishtadt, and A. A. Vasiliev, Physica D **141**, 281–296 (2000).
[38]V. I. Karpman, Space Sci. Rev. **16**, 361–388 (1974).
[39]V. I. Karpman, J. N. Istomin, and D. R. Shklyar, Plasma Phys. **16**, 685–703 (1974).
[40]Y. Katoh and Y. Omura, Geophys. Res. Lett. **34**, 3102, https://doi.org/10.1029/2006GL028594 (2007).
[41]Y. Katoh and Y. Omura, Geophys. Res. Lett. **34**, L13102, https://doi.org/10.1029/2006GL028594 (2007).
[42]C. F. Kennel and F. Engelmann, Phys. Fluids **9**, 2377–2388 (1966).
[43]C. F. Kennel and H. V. Wong, J. Plasma Phys. **1**, 75 (1967).
[44]G. V. Khazanov, A. A. Tel'nikhin, and T. K. Kronberg, J. Geophys. Res. **118**, 6397–6404, https://doi.org/10.1002/2013JA019122 (2013).
[45]G. V. Khazanov, A. A. Tel'nikhin, and T. K. Kronberg, Nonlinear Processes Geophys. **21**, 61–85 (2014).
[46]M. Kitahara and Y. Katoh, J. Geophys. Res. **124**, 5568–5583, https://doi.org/10.1029/2019JA026493 (2019).
[47]C. Krafft, A. S. Volokitin, and M. Flé, Phys. Plasmas **7**, 4423–4432 (2000).
[48]I. V. Kuzichev, A. R. Soto-Chavez, J. Park, A. Gerrard, and A. Spitkovsky, Phys. Plasmas **26**, 072901 (2019a).
[49]I. V. Kuzichev, I. Y. Vasko, A. Rualdo Soto-Chavez, Y. Tong, A. V. Artemyev, S. D. Bale, and A. Spitkovsky, Astrophys. J. **882**, 81 (2019).
[50]L. D. Landau and E. M. Lifshitz, *Mechanics. Course of Theoretical Physics* (Pergamon, Oxford, 1988), Vol. 1.
[51]I. Lerche, Phys. Fluids **11**, 2459 (1968).
[52]W. Li, J. Bortnik, R. M. Thorne, and V. Angelopoulos, J. Geophys. Res. **116**, 12205, https://doi.org/10.1029/2011JA017035 (2011).
[53]W. Li, J. Bortnik, R. M. Thorne, C. M. Cully, L. Chen, V. Angelopoulos, Y. Nishimura, J. B. Tao, J. W. Bonnell, and O. Lecontel, J. Geophys. Res. **118**, 1461–1471, https://doi.org/10.1002/jgra.50176 (2013).
[54]W. Li, D. Mourenas, A. V. Artemyev, J. Bortnik, R. M. Thorne, C. A. Kletzing, W. S. Kurth, G. B. Hospodarsky, G. D. Reeves, H. O. Funsten, and H. E. Spence, Geophys. Res. Lett. **43**, 8867–8875, https://doi.org/10.1002/2016GL070386 (2016).
[55]A. J. Lichtenberg and M. A. Lieberman, *Regular and Stochastic Motion* (Springer, 1983).
[56]L. R. Lyons and D. J. Williams, *Quantitative Aspects of Magnetospheric Physics* (Kluwer Academic Publishers, 1984).
[57]D. Mourenas, A. V. Artemyev, O. V. Agapitov, V. Krasnoselskikh, and F. S. Mozer, J. Geophys. Res. **120**, 3665–3683, https://doi.org/10.1002/2015JA021135 (2015).
[58]D. Mourenas, A. V. Artemyev, O. V. Agapitov, F. S. Mozer, and V. V. Krasnoselskikh, J. Geophys. Res. **121**, 4498–4517, https://doi.org/10.1002/2015JA022223 (2016).
[59]D. Mourenas, X. J. Zhang, A. V. Artemyev, V. Angelopoulos, R. M. Thorne, J. Bortnik, A. I. Neishtadt, and A. A. Vasiliev, J. Geophys. Res. **123**, 4979–4999, https://doi.org/10.1029/2018JA025417 (2018).
[60]A. Neishtadt, J. Appl. Math. Mech. **39**, 594–605 (1975).
[61]A. Neishtadt and A. Vasiliev, Nonlinearity **18**, 1393–1406 (2005).
[62]A. I. Neishtadt, "On adiabatic invariance in two-frequency systems," in *Hamiltonian Systems with Three or More Degrees of Freedom*, NATO ASI Series C, edited by C. Simo (Kluwer Academic Publishers, Dordrecht, 1999), Vol. 533, pp. 193–213.
[63]A. I. Neishtadt, Russ. Math. Surv. **69**, 771 (2014).
[64]B. Ni, R. M. Thorne, X. Zhang, J. Bortnik, Z. Pu, L. Xie, Zj Hu, D. Han, R. Shi, C. Zhou, and X. Gu, Space Sci. Rev. **200**, 205–259 (2016).
[65]D. Nunn, J. Plasma Phys. **6**, 291 (1971).
[66]D. Nunn and Y. Omura, J. Geophys. Res. **120**, 2890–2911, https://doi.org/10.1002/2014JA020898 (2015).
[67]Y. Omura, N. Furuya, and D. Summers, J. Geophys. Res. **112**, 6236, https://doi.org/10.1029/2006JA012243 (2007).
[68]Y. Omura, H. Matsumoto, D. Nunn, and M. J. Rycroft, J. Atmos. Terr. Phys. **53**, 351–368 (1991).
[69]Y. Omura, Y. Miyashita, M. Yoshikawa, D. Summers, M. Hikishima, Y. Ebihara, and Y. Kubota, J. Geophys. Res. **120**, 9545–9562, https://doi.org/10.1002/2015JA021563 (2015).
[70]R. Z. Sagdeev, D. A. Usikov, and G. M. Zaslavsky, *Nonlinear Physics. From the Pendulum to Turbulence and Chaos* (Harwood Academic Publishers, 1988).
[71]S. M. Shaaban, M. Lazar, P. H. Yoon, S. Poedts, and R. A. López, Mon. Not. R. Astron. Soc. **486**, 4498–4507 (2019).
[72]D. R. Shklyar, Sov. Phys. JETP **53**, 1197–1192 (1981).
[73]D. R. Shklyar and H. Matsumoto, Surv. Geophys. **30**, 55–104 (2009).
[74]Y. Y. Shprits, D. A. Subbotin, N. P. Meredith, and S. R. Elkington, J. Atmos. Sol.-Terr. Phys. **70**, 1694–1713 (2008).
[75]V. V. Solovev and D. R. Shkliar, Sov. Phys. JETP **63**, 272–277 (1986).
[76]R. L. Stenzel, J. Geophys. Res. **104**, 14379–14396, https://doi.org/10.1029/1998JA900120 (1999).
[77]T. H. Stix, *The Theory of Plasma Waves* (McGraw-Hill, 1962).
[78]D. Summers, R. M. Thorne, and F. Xiao, J. Geophys. Res. **103**, 20487–20500, https://doi.org/10.1029/98JA01740 (1998).
[79]X. Tao, J. Bortnik, J. M. Albert, and R. M. Thorne, J. Geophys. Res. **117**, 10205, https://doi.org/10.1029/2012JA017931 (2012).
[80]X. Tao, J. Bortnik, J. M. Albert, R. M. Thorne, and W. Li, J. Atmos. Sol.-Terr. Phys. **99**, 67–72 (2013).

[81]X. Tao, J. Bortnik, R. M. Thorne, J. M. Albert, and W. Li, Geophys. Res. Lett. **39**, 6102, https://doi.org/10.1029/2012GL051202 (2012).
[82]X. Tao, L. Chen, X. Liu, Q. Lu, and S. Wang, Geophys. Res. Lett. **44**, 8122–8129, https://doi.org/10.1002/2017GL074881 (2017).
[83]X. Tao, F. Zonca, and L. Chen, Geophys. Res. Lett. **44**, 3441–3446, https://doi.org/10.1002/2017GL072624 (2017).
[84]R. M. Thorne, Geophys. Res. Lett. **372**, 22107, https://doi.org/10.1029/2010GL044990 (2010).
[85]R. M. Thorne, W. Li, B. Ni, Q. Ma, J. Bortnik, L. Chen, D. N. Baker, H. E. Spence, G. D. Reeves, M. G. Henderson, C. A. Kletzing, W. S. Kurth, G. B. Hospodarsky, J. B. Blake, J. F. Fennell, S. G. Claudepierre, and S. G. Kanekal, Nature **504**, 411–414 (2013).
[86]R. M. Thorne, B. Ni, X. Tao, R. B. Horne, and N. P. Meredith, Nature **467**, 943–946 (2010).
[87]E. E. Titova, B. V. Kozelov, F. Jiricek, J. Smilauer, A. G. Demekhov, and V. Y. Trakhtengerts, Ann. Geophys. **21**, 1073–1081 (2003).
[88]Y. Tong, I. Y. Vasko, A. V. Artemyev, S. D. Bale, and F. S. Mozer, Astrophys. J. **878**, 41 (2019).
[89]B. T. Tsurutani, B. J. Falkowski, O. P. Verkhoglyadova, J. S. Pickett, O. Santolík, and G. S. Lakhina, J. Geophys. Res. **116**, 9210, https://doi.org/10.1029/2010JA016237 (2011).
[90]E. Tyler, A. Breneman, C. Cattell, J. Wygant, S. Thaller, and D. Malaspina, Geophys. Res. Lett. **46**, 2328–2336, https://doi.org/10.1029/2019GL082292 (2019).
[91]D. Vainchtein, X. J. Zhang, A. Artemyev, D. Mourenas, V. Angelopoulos, and R. M. Thorne, J. Geophys. Res. **123**, 8149–8169, https://doi.org/10.1029/2018ja025654 (2018).
[92]B. Van Compernolle, X. An, J. Bortnik, R. M. Thorne, P. Pribyl, and W. Gekelman, Phys. Rev. Lett. **114**, 245002 (2015).
[93]N. G. Van Kampen, *Stochastic Processes in Physics and Chemistry*, 3rd ed. (North Holland, 2003).
[94]A. Vasiliev, A. Neishtadt, and A. Artemyev, Phys. Lett. A **375**, 3075–3079 (2011).
[95]I. Y. Vasko, F. S. Mozer, V. V. Krasnoselskikh, A. V. Artemyev, O. V. Agapitov, S. D. Bale, L. Avanov, R. Ergun, B. Giles, P. A. Lindqvist, C. T. Russell, R. Strangeway, and R. Torbert, Geophys. Res. Lett. **45**, 5809–5817, https://doi.org/10.1029/2018GL077835 (2018).
[96]A. A. Vedenov and R. Z. Sagdeev, "Some properties of a plasma with an anisotropic ion velocity distribution in a magnetic field," in *Plasma Physics and the Problem of Controlled Thermonuclear Reactions*, edited by M. A. Leontovich (Pergamon Press, 1961), Vol. 3, p. 332.
[97]A. A. Vedenov, E. Velikhov, and R. Sagdeev, Nucl. Fusion Suppl. **2**, 465–475 (1962).
[98]P. Veltri, A. Mangeney, and J. D. Scudder, Nuovo Cimento C **15**, 607–619 (1992).
[99]P. Veltri and G. Zimbardo, J. Geophys. Res. **98**, 13335–13346, https://doi.org/10.1029/93JA01144 (1993).
[100]A. S. Volokitin and C. Krafft, Phys. Plasmas **8**, 3748–3758 (2001).
[101]A. S. Volokitin and C. Krafft, Phys. Plasmas **8**, 4960–4971 (2001).
[102]L. B. Wilson III, C. A. Cattell, P. J. Kellogg, J. R. Wygant, K. Goetz, A. Breneman, and K. Kersten, Geophys. Res. Lett. **38**, 17107, https://doi.org/10.1029/2011GL048671 (2011).
[103]L. B. Wilson III, A. Koval, A. Szabo, A. Breneman, C. A. Cattell, K. Goetz, P. J. Kellogg, K. Kersten, J. C. Kasper, B. A. Maruca, and M. Pulupa, Geophys. Res. Lett. **39**, 8109, https://doi.org/10.1029/2012GL051581 (2012).
[104]P. H. Yoon, V. S. Pandey, and D. H. Lee, Phys. Plasmas **20**, 112902 (2013).
[105]X. Zhang, V. Angelopoulos, A. V. Artemyev, and J. Liu, Geophys. Res. Lett. **45**, 9380–9389, https://doi.org/10.1029/2018GL079613 (2018).
[106]X. J. Zhang, D. Mourenas, A. V. Artemyev, V. Angelopoulos, J. Bortnik, R. M. Thorne, W. S. Kurth, C. A. Kletzing, and G. B. Hospodarsky, Geophys. Res. Lett. **46**, 7182–7190, https://doi.org/10.1029/2019GL083833 (2019).
[107]X. J. Zhang, R. Thorne, A. Artemyev, D. Mourenas, V. Angelopoulos, J. Bortnik, C. A. Kletzing, W. S. Kurth, and G. B. Hospodarsky, J. Geophys. Res. **123**, 5379–5393, https://doi.org/10.1029/2018JA025390 (2018).